Asymmetric synchronization in lattices of pinned spiral waves

Franco M. Zanotto and Oliver Steinbock*
Florida State University, Department of Chemistry and Biochemistry, Tallahassee, Florida 32306-4390, USA

(Received 15 October 2020; accepted 3 February 2021; published 22 February 2021)

Networks of coupled oscillators show a wealth of fascinating dynamics and are capable of storing and processing information. In biological and social networks, the coupling is often asymmetric. We use the chirality of rotating spiral waves to introduce this asymmetry in an excitable reaction-diffusion model. The individual vortices are pinned to unexcitable disks and arranged at a constant spacing L along straight lines or simple geometric patterns. In the case of periodic boundaries or pinning disks arranged along the edge of a closed shape, small L values lead to synchronization via repeated wave collisions. The rate of synchronization as a function of L shows a single maximum and is determined by the dispersion behavior of a continuous wave train traveling along the system boundary. For finite systems, spirals are affected by their upstream neighbor, and a single dominant spiral exists along each chain. Specific initial conditions can decouple neighboring vortices even for small L values. We also present a time-delay differential equation that reproduces the phase dynamics in periodic systems.

DOI: 10.1103/PhysRevE.103.022213

I. INTRODUCTION

Networks of coupled oscillators display a plethora of interesting dynamics and synchronization phenomena [1,2]. Examples include the classic self-synchronization of light-signaling fireflies [3] and biological cells responsible for the generation of circadian rhythms [4]. Partial synchronization can induce the formation of so-called chimeras, which sustain synchronous and asynchronous behavior simultaneously [5,6]. Of importance for all of these phenomena are the network topology, which can include regular and random as well as scale-free and small-world networks [7–9]. Quite naturally, the intrinsic dynamics of each node also play an important role, and much attention has been dedicated to linear, limit-cycle, and chaotic oscillators [10,11]. The third important ingredient is the coupling strength w_{ij} between the connected nodes i and j, which in the simplest case can be constant (for $i \neq j$). In neuronal networks, these parameters can encode holographic memory and usually obey $w_{ij} = w_{ji}$ [12]. Most experimental systems, however, do not obey this symmetric coupling criterion. For example, in a social network a celebrity or influencer will affect followers more strongly than the followers affect the celebrity. Also for biological cells, asymmetric coupling is a well-established phenomenon. Numerous publications document this "rectification" for electrical synapses in crayfish [13], the giant fiber system in *Drosophila* [14], spinal cord preganglionic neurons [15], and many other examples. Furthermore, non-neuronal cells can show asymmetric communication as exemplified by oocytes of the frog *Xenopus* [16].

The goal of this study is to introduce a nonlinear reaction-diffusion system that can generate asymmetric coupling between network oscillators with only minimal external intervention and that is suitable for future experimental studies. For this purpose, we consider a population of rotating spiral waves pinned to a static lattice of stationary and inert heterogeneities. Spiral waves of excitation exist in numerous experimental systems such as the chemical Belousov-Zhabotinsky (BZ) reaction [17], catalytic surface reactions [18], vegetation patterns in high-altitude wetlands [19], and cardiac as well as neuronal tissue [20,21]. Excitation waves propagate with a constant amplitude due to the domino-chain-like spread of the excitation. Figuratively, these dominoes are lifted up again by slower processes that introduce a refractory zone in the wake of the front. The resulting constant (and system-specific) front speed c_0 is lowered by a tight spacing of fronts and also by concave deformations of the front curve that effectively dilute the often diffusion-mediated spread of the excitation [22]. Excitation waves typically show no interference and no reflection at boundaries.

Free spiral waves rotate with a characteristic frequency that is typically lowered if the spiral tip is forced to orbit around an inactive heterogeneity [23]. For disk-shaped heterogeneities of increasing size, the frequency quickly converges to the ratio of the boundary circumference and the constant wave speed c_0. Pinned excitation vortices have been reported for cellular automata [24], numerous reaction-diffusion models [23], and experimental systems including the BZ reaction [25]. In this chemical system, heterogeneities were generated by laser light [25], catalyst-free regions [26], and physical obstacles created by inclusion of inert and impermeable objects [27] as well as soft-lithography [28]. Pinning of excitation vortices is also possible for spatially three-dimensional systems in which excitation vortices rotate around one-dimensional space curves [29].

II. MODEL AND METHODS

The geometry of our model aims to describe the spiral waves generated in a catalyst-loaded polysulfone membrane

*osteinbock@fsu.edu

(or similar host media, such as a gel) submerged in a catalyst-free solution of BZ reactants [26]. Notice that the catalyst is immobilized and does not diffuse. These membranes could be perforated to create pinning sites and optionally attached to glass cylinders to yield a ribbon-shaped system. The simulations presented herein are based on the two-dimensional Barkley model of excitable systems [30]. This model considers an activator u and an inhibitor v, of which only u is able to diffuse. The evolution of these variables is described by the following equations:

$$\frac{\partial u}{\partial t} = \nabla^2 u + \frac{1}{\epsilon}\left[u(1-u)\left(u - \frac{v+b}{a}\right)\right], \tag{1}$$

$$\frac{\partial v}{\partial t} = u - v, \tag{2}$$

where ϵ, a, and b are dimensionless constants. Throughout this work, these parameters were set as $\epsilon = 0.02$, $a = 0.90$, and $b = 0.05$. All lengths and times are expressed using dimensionless units. For the given parameters, unpinned spiral waves exist and the spiral tip describes a small circular trajectory. To study the possible synchronization of spiral waves pinned to heterogeneities, a two-dimensional (2D) simulation domain was prepared with specific characteristics.

For a linear chain of pinned spirals, the domain is rectangular in shape, with a height of L and a width of $n \times L$, where n is the number of spiral waves to be considered. Each pinning site is a circular heterogeneity of the system, in which u and v are fixed at 0. No-flux boundaries should create dynamics that are nearly identical to the results reported in this study, although the spiral tip will revolve at a closer distance and hence show a slightly decreased rotation period. The unexcitable disks are spaced at a center-to-center distance of L and have a radius r that is larger than the radius of the free spiral tip trajectory. The upper and lower border of the system domain obey no-flux boundary conditions in every case. Furthermore, the left and right limits are periodic boundaries in the cases presented in Sec. III A and no-flux boundaries in Sec. III C. Accordingly, the system is a closed ribbon in the former case and a wide rectangle in the latter.

For an arrangement of spirals on a square, unexcitable disks are also included, separated by a distance of L, in a domain of size $2L \times 2L$ in one case and $3L \times 3L$ in the other, with four and eight disks, respectively. In these cases, all sides of the domain obey no-flux boundary conditions.

Spiral waves are initialized by setting $u = 0$ and $v = 0$ everywhere in the system except for thin bands that join each of the disks with the outer system boundary. Within these bands, the value of u is set according to a Gaussian function around the center of the band. The value of v is set in the same way, with a slight shift toward either the left or the right. The direction of this shift gives the wave a clockwise or anticlockwise sense of rotation. The angle between these bands and the positive x direction is varied as an initialization parameter.

III. RESULTS AND DISCUSSION

A. Spiral waves arranged on closed ribbons

For most of our analyses, all spirals are pinned to unexcitable disks of the same radius. Accordingly, these spirals have identical frequencies if left unperturbed by their neighbors. The spiral wavelength Λ increases linearly with increasing disk radii r. Around the investigated value of $r = 5.0$, $\Lambda(r)$ is linear with a slope of 6.90 and an intercept of 8.32. The slope is close to the expected, simple value of 2π (the source of deviation is discussed in Ref. [31]). Additionally, simulations confirmed that the wave propagation speed is independent of r for $r > 3.0$.

An important variable that allows for the quantitative analysis of the synchronization behavior is the phase angle of each spiral wave, ϕ. This value is defined as the angle between the horizontal axis and the segment that connects the center of the disk to the tip of the spiral. The tip of the wave is determined as the intersection of the isolines for $u = 0.3$ and $v = 0.3$. This intersection point, marked in the examples in Fig. 1 with a cross, is unique for each spiral. If a pinned wave is left to evolve unperturbed by its neighbors, its phase value will increase (for counterclockwise rotation) or decrease (for clockwise rotation) at a constant rate ω. This value presents a linear relationship with respect to r for $r > 3.0$. The most relevant geometric parameters that the model allows to modify are r, L, and n. A radius of 5.0, which corresponds to $\Lambda = 42.8$, was used for the simulations presented below, and n was limited to a maximum of 4.

Beyond these geometric factors, we also vary parameters such as the chirality along the vortex chain and the initial phase values of the spirals. Both of these factors drastically influence the system's synchronization behavior. We specifically consider the two cases in which the initial phase of neighboring spirals is similar or differs by approximately π. Figures 1(a)–1(d) illustrate these combinations for the simplest case of $n = 2$. The snapshots in Figs. 1(a) and 1(b) also emphasize the importance of wave collisions, which effectively shield the spiral tips and prevent a mutual coupling and ultimately synchronization. Figures 1(e)–1(i) show vector fields that represent the direction of wave motion at select points in space. Panels (e) and (f), which correspond to the waves shown in panels (a) and (b), reveal that the simulation domain is divided by two separatrices, which extend along the lines of wave collisions. These separatrices function as a clear indicator of whether synchronization behavior is possible for a given geometry and set of initial conditions. Importantly, this statement holds for more complicated geometries and arrangements of heterogeneities.

The situation in Fig. 1(g), which corresponds to the wave in panel (c), is qualitatively different. Here, the lines of wave collisions connect the upper and lower system boundary to the unexcitable disks and, hence, do not define distinct regions. This scenario and the underlying wave behavior lead to interaction between the spiral tips and open up the possibility for synchronization. The importance of the disk distance L is illustrated by the vector fields in Figs. 1(h) and 1(i). In these examples, both waves rotate clockwise and start from the same phase value as in panel (d), but they have different values of L. Notice the disparate scales of the two panels. In general, we find distinct behavior for L values above and below Λ. In panel (h) ($L = 60$), the domain is again divided into halves. This is the general case for $L > \Lambda$ and does not allow for synchronization. In contrast, panel (i) ($L = 30$) has no wall-to-wall separatrices, and parallel wave fronts can travel continuously within the the lower portion of the system.

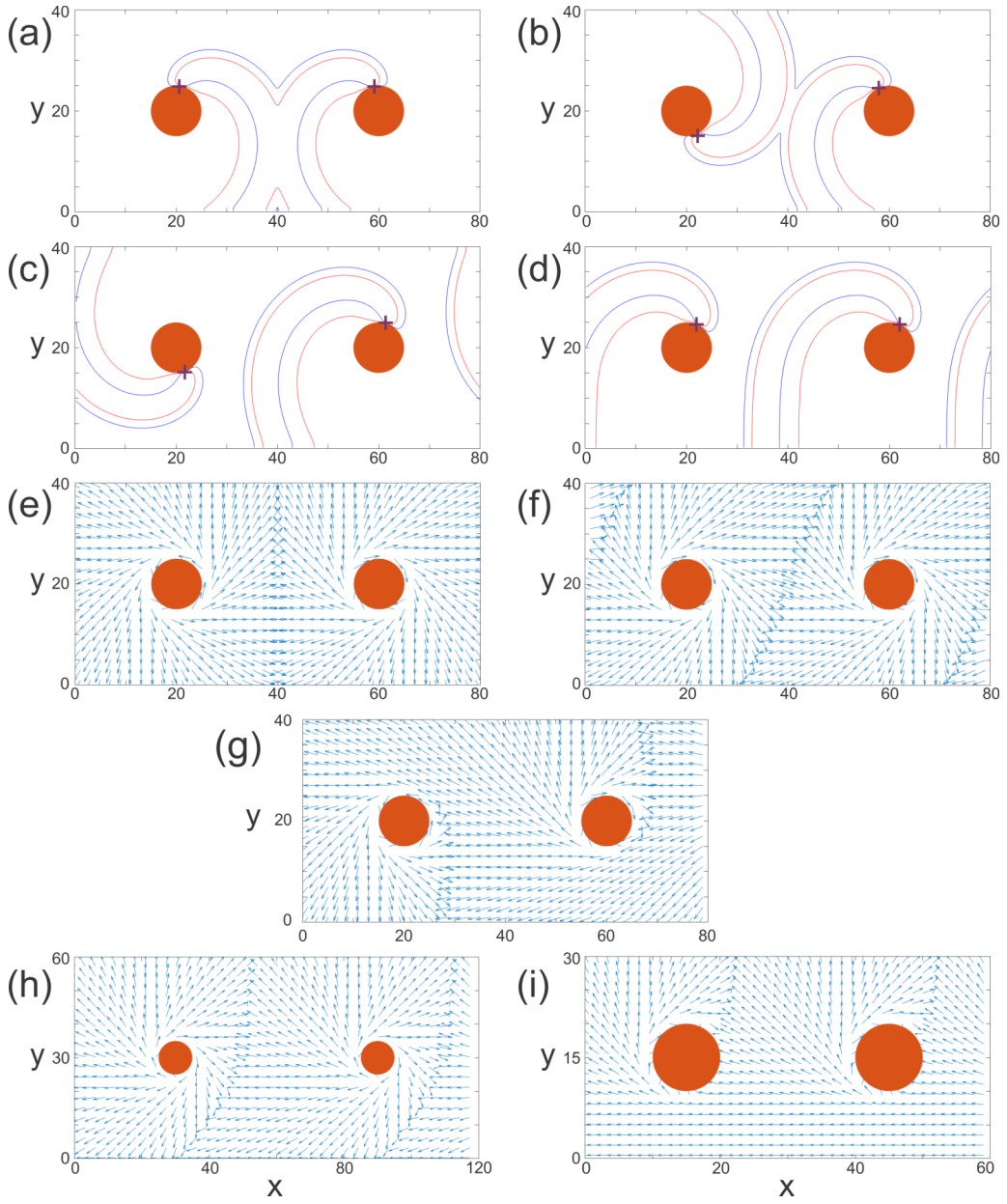

FIG. 1. (a)–(d) Representative snapshots for spiral waves pinned to two adjacent unexcitable disks. The upper and lower domain boundaries impose no-flux conditions, while the left and right borders are periodic boundaries. The circles represent unexcitable regions. The blue (leading) isoline corresponds to $u = 0.3$ and the red (trailing) isoline corresponds to $v = 0.3$. Each panel corresponds to a different rotation direction and starting position. (e)–(i) Vector fields showing the propagation direction at each point. (a) and (e) $L = 40$, counterclockwise and clockwise rotating spirals; both waves are started in the lower half of the simulation domain. (b) and (f) $L = 40$, clockwise rotating spirals; each of the waves is started within opposite sides of the domain. (c) and (g) $L = 40$, counterclockwise and clockwise rotating spirals; each of the waves is started at opposite sides of the domain. (d), (h), and (i) Clockwise rotating spirals; both waves are started on the lower half of the simulation domain, with $L = 40$ (d), $L = 60$ (h), and $L = 30$ (i). Animations corresponding to panels (e)–(i) are included in the supplemental material [Movies 1(a)–1(e)] [32].

As these dynamics are easier to understand from animations, we refer the reader to the videos in the supplemental material (Movie 1) [32].

We analyze the temporal dynamics of the latter two cases in terms of a relative phase, which we define as the difference between the phase of the ith vortex, ϕ_i, and the mean phase ($\overline{\phi} = \sum_{i=1}^{n} \phi_i/n$). Corresponding data are shown in Fig. 2, where panel (a) is representative of all cases with $L > \Lambda$. This panel shows the ϕ_i values of the two spirals evolving independently with the same angular velocity ω. This behavior reveals that the vortices do not interact but are rather shielded by their sufficiently long wave arms. In contrast, Fig. 2(b) shows the corresponding plot for a pair of interacting spiral tips that undergo abrupt phase resets due to collisions of a given wave arm with the neighboring heterogeneity. This example is representative for $L < \Lambda$. Surprisingly, both vortices alternate between two relative phase values, forming a braidlike pattern in the respective phase evolution curves.

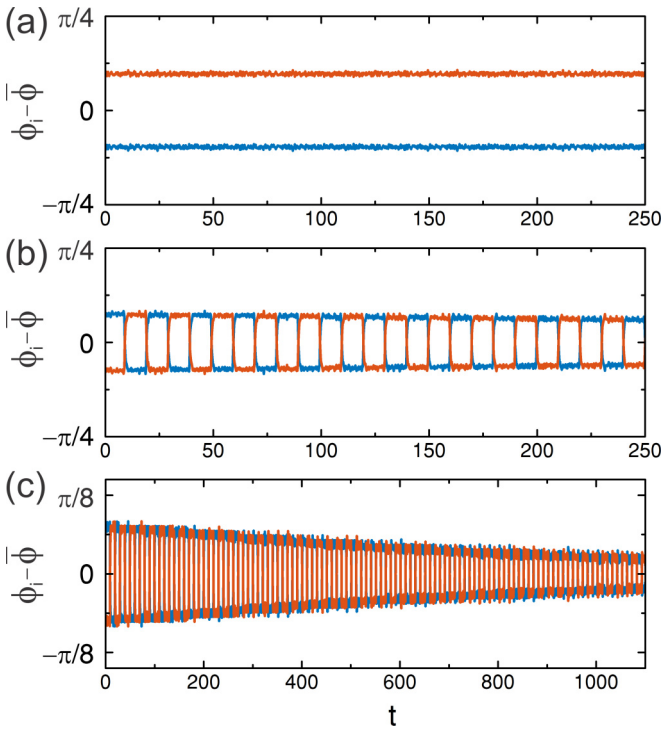

FIG. 2. Relative phase of each spiral as a function of time. (a) $L = 60$ and (b,c) $L = 40$.

Accordingly, the roles of phase-leading and phase-lagging rotors also alternate with a constant period. An animation showing the corresponding wave dynamics is presented in the supplemental material (Movie 2) [32]. While the braidlike functions in Fig. 2(b) seem nearly of constant amplitude, long simulation times reveal synchronization to a relative phase of zero. This long-term process is illustrated in Fig. 2(c) as an extension of the data in (b). We note that both braidlike phase dynamics and synchronization are also found for larger values of n, as long as $L < \Lambda$.

The mechanism for this synchronization can be rationalized in terms of the underlying dispersion relation [33,34], i.e., the speed-wavelength dependence of the excitable system. The resulting dynamics in the band of continuous wave propagation below (or on top of) the heterogeneities are strongly dominated by this dispersion relation. Here, n wave pulses propagate in the same direction, but with initially nonconstant spacing. In many chemical systems as well as in the investigated Barkley model, these wave pulses will differ in speed c depending on the distance λ to the pulse ahead of them because the latter leaves the local system in a state of partial refractoriness. The monotonically increasing nature of $c(\lambda)$ (normal dispersion) ultimately causes the wave train to establish a constant pulse distance, and, in the process, it also synchronizes the spiral rotors. To illustrate this hidden mechanism, we reduce the system to a one-dimensional domain of length nL while maintaining periodic boundary conditions at the edges, and we position three wave fronts with initially nonequidistant spacings. Figure 3(a) shows the corresponding $u(x)$ and $v(x)$ profiles for an early and a late time as blue (solid) and red (dashed) curves, respectively. The collective deviation from the final state can be quantified by defining the variable $\Upsilon(t)$ as

$$\Upsilon(t) = \sum_{i=1}^{n} |\lambda_i(t) - L|, \tag{3}$$

where λ_i is the peak-to-peak distance between consecutive wave fronts. A value of $\Upsilon = 0$ indicates that the waves are equidistant.

Figure 3(b) shows the temporal evolution of Υ for $n = 3$ and different values of L. The initial front distances are $L - 2.5$, $L + 5.0$, and $L - 2.5$. As the simulation domain is increased in size, the peak-to-peak distances grow and the speed differences between the pulses decrease according to the saturating dispersion relation $c(\lambda)$. Figure 3(c), in turn, shows the same plot for the 2D system with three pinned waves. In this case, λ_i is defined as the peak-to-peak distance between the nearly parallel wave fronts that travel along the bottom boundary of the domain [see Fig. 1(i)]. For relatively low values of L, the graphs in (b) and (c) show very similar behavior. However, as the value of L approaches Λ, the shapes of the graphs differ drastically, showing in some cases abrupt changes in slope. From each of these graphs, a value of $t_{1/2}$ can be extracted. This value is defined as the time needed for Υ to reach half of its initial value. Figure 3(d) shows how this value depends on L for the data in Figs. 3(b) and 3(c). In the case of the 1D model, $t_{1/2}$ increases monotonically with L. The behavior for pinned spirals is initially similar, but $t_{1/2}$ reaches a maximum (slowest synchronization) at $L \approx 38$. For higher L values, the synchronization of the spirals occurs again more rapidly, but above 46, synchronization does not occur at all. Notice that the wavelength $\Lambda = 42.8$ of the pinned spirals is within the range of accelerating synchronization. The most important observation in this context is the existence of an apparent resonance effect.

B. Time-delay differential equation

Time-delay differential equations are useful for the description of certain complex systems and especially of those involving feedback control, such as automatic engines or physiological systems [35]. Additionally, they have been used to capture nonlinear chemical kinetics [36–38]. We formulate a system of delay differential equations to describe the behavior of a group of pinned spiral waves arranged on a periodic $1 \times n$ lattice. From the numerical results in Sec. III A, it can be stated that $\phi_i(t)$ evolves by means of only one of two mechanisms. The trivial case is a gradual increase with rate ω as the wave center rotates independently around its anchoring disk. The second case involves sudden phase changes due to collisions with one adjacent wave arm. In the following, we will assume—without loss of generality—that all spirals rotate clockwise (decreasing phases) and that each spiral i is subject to perturbations by its right neighbor $i + 1$ due to wave collision.

To incorporate these sudden phase changes of ϕ_i into a differential equation, and to describe the overall dynamics, we consider

$$\frac{d\phi_i(t)}{dt} = \omega + A\delta(\theta), \tag{4}$$

$$\delta(\theta) = \delta\left\{\left[\phi_{i+1}\left(t - \frac{L}{c}\right) \mod 2\pi\right] - \phi_B\right\}, \tag{5}$$

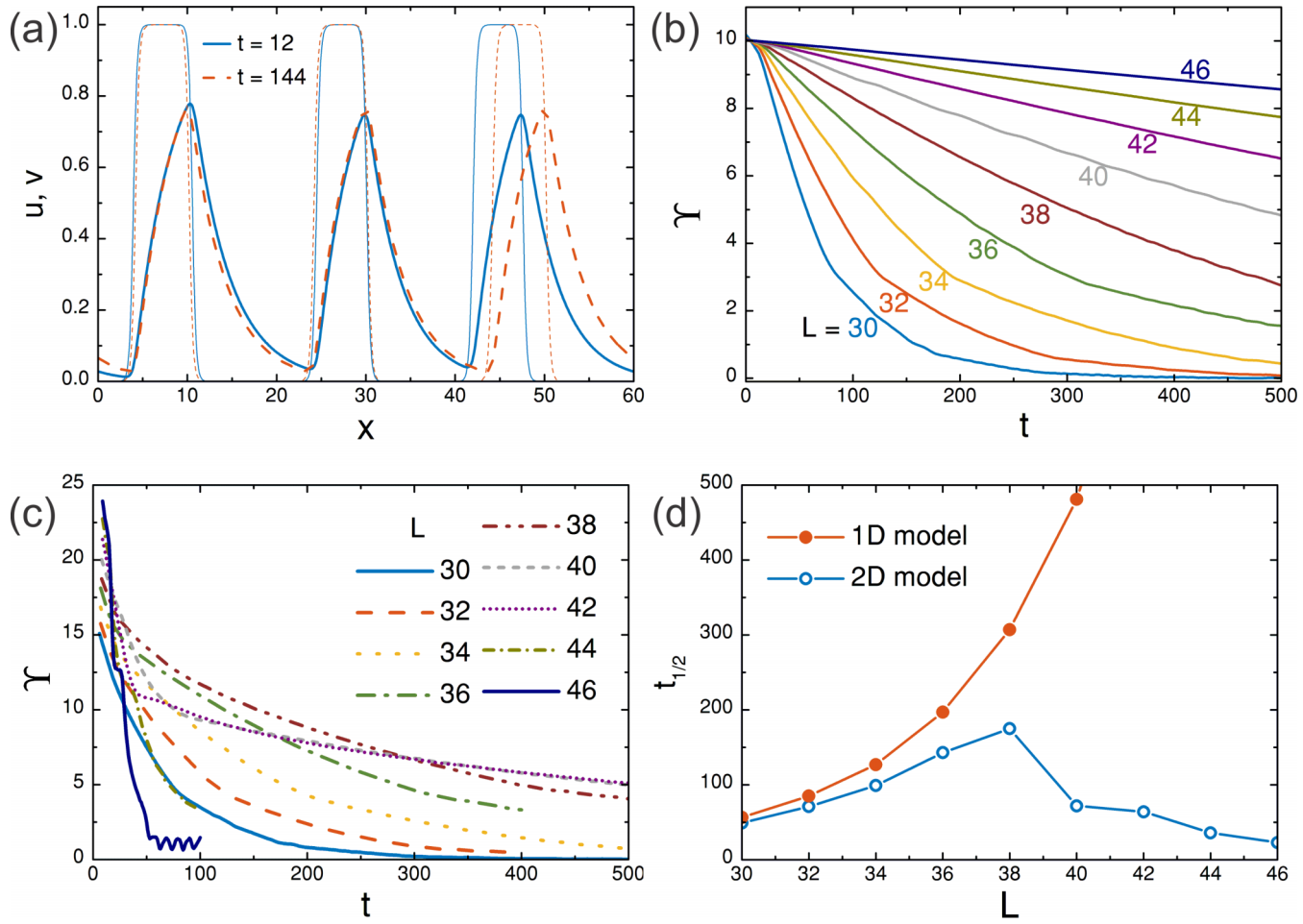

FIG. 3. (a) u (thin lines) and v (thick lines) as a function of x for the 1D model, corresponding to an early stage ($t = 12$, solid blue lines) and a later stage ($t = 144$, dashed red lines), showing the evolution of a wave train toward equidistant waves. (b) $\Upsilon(t)$ for different values of L according to the 1D model. (c) $\Upsilon(t)$ for different values of L according to the 2D model with unexcitable disks. (d) $t_{1/2}$ as a function of L, corresponding to the simulations shown in panels (b) and (c).

where θ is an auxiliary variable, A is an amplitude, and $\phi_B = 3\pi/2$. The value of ϕ_B describes the phase value at which the collision-induced phase reset occurs (the lowest position of the spiral tip with respect to Fig. 1). The function $\delta(\theta)$ must satisfy two conditions: (i) δ must fall off quickly when departing from $\theta = 0$ to achieve a sufficiently fast phase jump, and (ii) its integral must be equal to 1. The expression for the variable θ involves the time L/c that the wave needs to travel the distance L between neighboring pinning sites. This value is the delay constant of our model. Finally, θ is chosen so that the maximal phase reset occurs when its neighboring rotor $i+1$ had reached ϕ_B at a time L/c earlier. In addition, the modulo function is used to account for the motion of the tip along a circle.

Notice that the period of the system is shortened from the single rotor period $T = 2\pi/\omega$ to L/c. Considering an instantaneous phase reset, the reduction factor for the period is $\xi = (2\pi - A)/2\pi$ since A is the amplitude of the phase jump. Accordingly, we find that $\xi T = L/c$ and hence that the amplitude is $A = 2\pi - \omega L/c$. In addition to this, a correction must be made to account for the phase difference between waves i and $i+1$. If wave i lags behind, then A will be higher, and if wave $i+1$ lags behind, the wave front will arrive later, leading to a smaller increase in phase. $\phi_i(t) - \phi_{i+1}(t)$ cannot be taken as a measure of this difference because it is likely that by time t, ϕ_{i+1} has been influenced by the wave pinned to disk $i+2$, so a previous time value should be chosen, such as $t - \frac{L}{2c}$. As a consequence,

$$A = 2\pi - \frac{\omega L}{c} + \phi_i\left(t - \frac{L}{2c}\right) - \phi_{i+1}\left(t - \frac{L}{2c}\right). \quad (6)$$

Equation (4) can then be written as

$$\frac{\partial \phi_i(t)}{\partial t} = \omega + \left[2\pi - \frac{\omega L}{c} + \phi_i\left(t - \frac{L}{2c}\right) - \phi_{i+1}\left(t - \frac{L}{2c}\right)\right] \times \delta\left\{\left[\phi_{i+1}\left(t - \frac{L}{c}\right) \mod 2\pi\right] - \phi_B\right\}. \quad (7)$$

Equation (7) can be solved numerically with a suitable choice of δ to predict the relative phase values as a function of time. It should be noted that the dispersion relation, which was identified above as the source for the synchronization behavior, is not taken into account by this description (c is constant), and, as a consequence, results are expected to differ from the direct simulations based on Eqs. (1) and (2) in the long run.

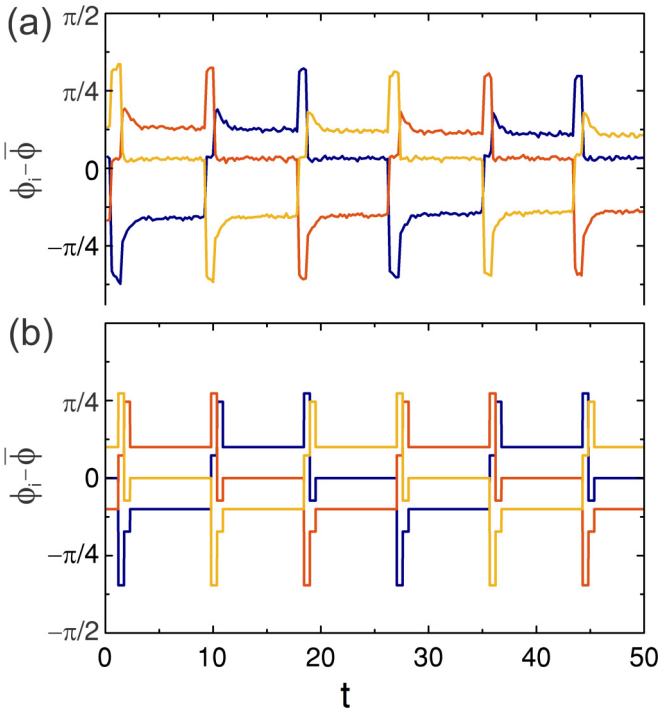

FIG. 4. Relative phase as a function of time for three pinned spiral waves. (a) Results corresponding to the Barkley model simulation. (b) Results corresponding to Eq. (7).

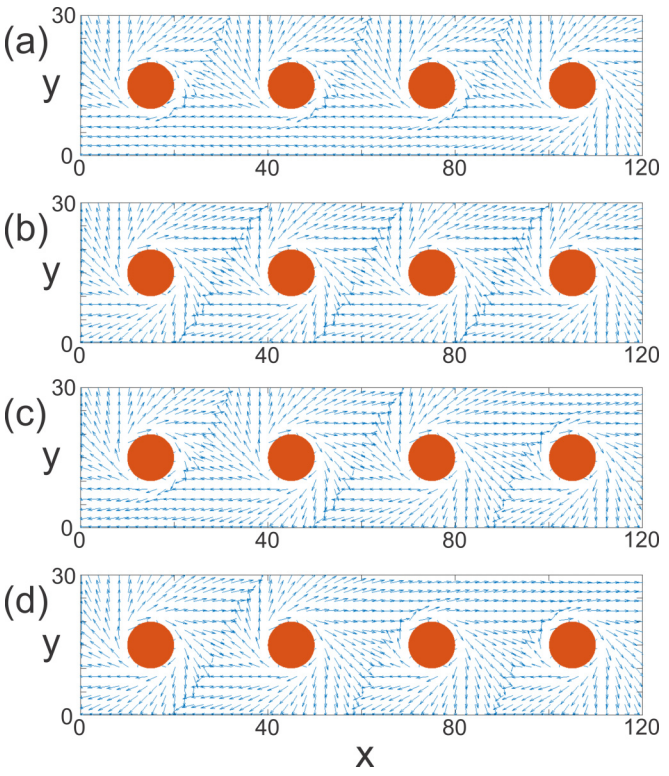

FIG. 5. Vector fields showing the propagation direction at each point for domains with nonperiodic boundaries. Each panel corresponds to different initial conditions. All waves rotate clockwise. $L = 30$. (a) All waves are initialized on the lower half of the simulation domain. (b) Waves are initialized in an alternated way above and below the midline of the simulation domain. (c) The two leftmost waves are initialized in the lower half of the simulation domain, while the rest are initialized in the upper half of the simulation domain. (d) The leftmost wave is initialized in the lower half of the simulation domain, while the rest are initialized in the upper half of the simulation domain.

To compare these results with the Barkley model simulations, we integrate Eq. (7) using the forward Euler method for $n = 3$ and $r = 5.0$. The values for ω and Λ are obtained from a simulation with a single spiral wave and a large enough value of L ($L > \Lambda$). A boxcar function with a width of $\omega\Delta t$ and a height of $A/(\omega\Delta t)$ was chosen as δ, where Δt is a single time step. The comparison of results from simulations [Fig. 4(a)] and the solution of Eq. (7) [Fig. 4(b)] shows a clear correspondence between the predicted relative phase and the value extracted from direct simulations. Equation (7) is able to reproduce both the correct timing between sudden increases in ϕ and the correct amplitude of each jump. It is also generalizable to any value of n, r, and $L < \Lambda$.

It should be noted that the description of the individual phases by means of this equation only requires the knowledge of geometrical aspects of the expanding spirals. These aspects are essentially independent of the particular reaction-diffusion model chosen to describe their evolution and of the physical basis of their formation. This implies that this treatment can be generalized to any excitable system capable of producing rotating spiral waves. In addition, the reduction in the degrees of freedom that accompanies the analysis of reaction-diffusion by a delay differential equation has allowed us to gain physical insight into the essential parameters needed to produce and describe this behavior.

C. Spiral waves arranged along a finite line

We performed additional simulations replacing the periodic boundary conditions with no-flux boundaries, and we found distinctly different coupling dynamics. Under these conditions and for equal chiralities, either the leftmost or the rightmost spiral invariably remains unperturbed due to the absence of an upstream wave. This master spiral exerts its influence over all points within the simulation domain if no wall-to-wall separatrices exist. All phases are determined by the master, and next-neighbor phase differences depend only on their respective spacing. As discussed before, the existence of wall-to-wall separatrices depends not only on the spacing L, but also on the initial phases. This feature is illustrated in Fig. 5.

Figure 5(a) shows the vector field of local wave directions for a case in which the rightmost wave determines the frequency and phase of all other waves. The initial conditions are $L < \Lambda$, clockwise rotation sense for each spiral and wave initialization in the lower half of the system (initial phase around $3\pi/2$). If the sense of rotation is reversed, or if the waves are initialized in the upper half of the system, the leftmost wave becomes dominant. If both of these changes are applied together, the rightmost wave becomes dominant again.

Wall-to-wall separatrices can be introduced by modifying only the initial state, and thus independent regions within the system arise. Each of these independent regions follows the

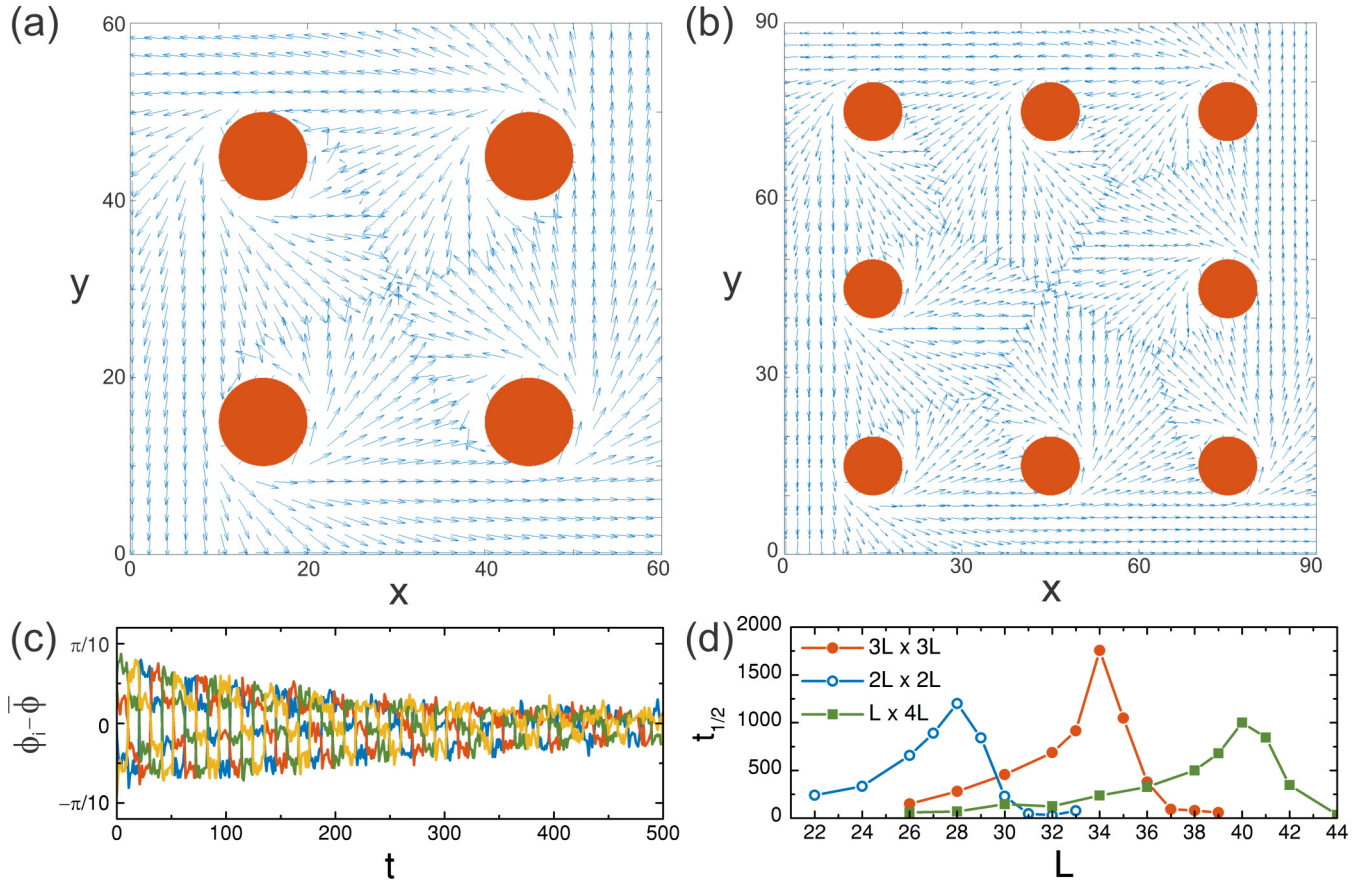

FIG. 6. (a),(b) Vector fields showing the propagation direction at each point for spiral waves pinned to four unexcitable disks arranged in a square in a $(2L \times 2L)$-sized domain (a) and a $(3L \times 3L)$-sized domain (b). All boundaries present no-flux conditions. $L = 30$. (c) Relative phase as a function of time corresponding to the geometry shown in panel (a). ϕ_i values are corrected for the $\pi/2$ rotation originated from the fourfold symmetry of the domain. (d) $t_{1/2}$ as a function of L, corresponding to $(2L \times 2L)$- and $(3L \times 3L)$-sized domains. Animations corresponding to panels (a) and (b) are included in the supplemental material [Movies 3(a) and 3(b)] [32].

same rules as mentioned before, where the upstream spiral determines the frequency and phase of the rest of the waves within its region. In Fig. 5(b) [as in the case of Fig. 1(f)], each spiral has its own region, resulting in noninteracting waves. In Figs. 5(c) and 5(d), the domain is divided into two regions by maintaining the clockwise sense of rotation for all waves, while initializing either two [Fig. 5(c)] or three [Fig. 5(d)] vortices in the upper half of the system. In the case of Fig. 5(c), this results in the second and third waves becoming dominant in their subdomains. In Fig. 5(d), the first (leftmost) spiral is the only one in its own region, and the second wave determines the phase of the third and fourth waves.

D. Spiral waves arranged on simple lattices

A straightforward way to avoid the existence of a dominant spiral without the use of periodic boundary conditions is to arrange the pinning disks along the edge of a closed shape, such as a square. Figures 6(a) and 6(b) illustrate examples for squares of size $2L \times 2L$ and $3L \times 3L$, respectively. These vector fields show the continuous propagation of waves along the outer edges of the domain. Although these systems share many of the characteristics of those in Sec. III A, the presence of 90° corners brings forth some additional features. First, the wave fronts responsible for the synchronization are not parallel at all times, as was seen in the previous cases. As a consequence, dispersion effects are weaker, and a longer time is required for synchronization to occur. Secondly, the presence of corners requires that the wave fronts travel longer distances between consecutive disks. This translates into a reduction of the maximum L value that allows for interaction between wave centers. As a consequence, $L < \Lambda$ stops being a useful criterion for assessing whether synchronization can occur. Thirdly, in the case of a $3L \times 3L$ (or larger) domain [Fig. 6(b)], a qualitative distinction arises between disks that occupy the corner positions and those positioned along the sides. While the former behave like those in the basic $2L \times 2L$ arrangement [Fig. 6(a)], the latter behave similarly to the ribbons discussed in Sec. III A.

As shown in the plot of $\phi_i(t) - \overline{\phi}(t)$ in Fig. 6(c), the braidlike behavior observed for periodic linear systems can also be encountered for unexcitable disks along the sides of a square. This specific example is obtained for a 60×60 domain with four pinning sites, i.e., the situation in Fig. 6(a). The graph also shows the long-term synchronization behavior. The underlying events are essentially identical to those

causing the braidlike phase dynamics for closed ribbons (Fig. 2).

Lastly, Fig. 6(d) shows the synchronization half-lives $t_{1/2}$ as a function of L for three different configurations, namely the original closed ribbon data (green squares), the $3L \times 3L$ square (full red circles), and the $2L \times 2L$ square (hollow blue circles). The curves are similar to each other, but—compared to the closed ribbon—the data for the square arrangements are shifted to lower L values. We conclude that resonance is achieved for lower values of L if disks are arranged along closed paths with 90° turns. This effect is less pronounced for the $3L \times 3L$ square, where corner sites make up only a fraction of the disks. In addition, we find that the largest L values for which synchronization can occur also shift in the same way. The specific values are $L = 33$, 39, and 45 for the $2L \times 2L$, $3L \times 3L$, and linear systems, respectively.

IV. CONCLUSIONS

Pinned spiral waves in excitable systems are chiral oscillators that can interact with nearby counterparts and potentially phase-synchronize. The coupling between interacting vortex pairs is reliably asymmetric and hence introduces interesting features such as position-dependent masters and slaves. In addition to the specific chiralities and distances, the initial phases of the spiral waves affect whether adjacent waves are able to interact. For systems with periodic features (ribbonlike chains or closed 2D paths), dominant oscillators do not arise and the population synchronizes due to a circulatory wave train and its specific dispersion behavior. The sometimes long-lived transients toward the synchronized state show unexpected dynamics which create braidlike features in the phase evolution curves. In addition, we found that the synchronization times vary with vortex distance and can show a single maximum. This maximum is the result of two opposing trends: as the distance increases, dispersion effects become weaker, delaying synchronization; at the same time, an apparent resonance effect greatly accelerates synchronization as the center-to-center distance approaches the intrinsic wavelength of the pinned spirals.

The pinned vortex chains and lattices analyzed in this study are suitable for experimental realizations with chemical systems such as the Belousov-Zhabotinsky reaction. For example, this reaction can be carried out in thin, catalyst-loaded polysulfone membranes submerged in a catalyst-free solution of BZ reactants [26]. These membranes could be perforated to create pinning sites and attached to glass cylinders to yield a ribbon-shaped system. Various experimental protocols for the initiation of pinned vortices have also been reported for this reaction. Unlike our simulations, the radius and position of the pinning sites will likely show small deviations from a constant value. We performed additional calculations to evaluate the effect of such variations, and we found that the phenomena described here continue to exist as long-lived transients. After sufficiently long times, however, the highest frequency spiral (smallest pinning site) becomes the dominant pacemaker and eventually establishes its frequency throughout the entire system [39,40].

The main idea of this study was to explore pinned spiral waves as phase oscillators with tunable, asymmetric coupling. The presented examples allowed us to establish basic rules, but clearly more complex geometries can be studied including vortex chains on closed Möbius bands and pinning site arrangements with branching points as well as irregular structures. Also, the shape of the individual spiral anchors could be varied to introduce anisotropies, for instance through elliptical pinning sites. Since the synchronization dynamics depend on the system's dispersion relation, we expect that excitable media with anomalous dispersion [41] will create even richer dynamics. Lastly, one can envision extensions to three-dimensional systems where rotating scroll waves readily pin to inert cylinders and tori [29]. In such three-dimensional cases, each rotor has the ability to encode a range of phases that would manifest themselves as a twist of the wave pattern.

ACKNOWLEDGMENT

This material is based upon work supported by the National Science Foundation under Grant No. 1565734.

[1] S. H. Strogatz, *Sync: The Emerging Science of Spontaneous Order* (Hyperion, New York, 2003).

[2] A. Pikovsky, M. Rosenblum, and J. Kurths, *Synchronization: A Universal Concept in Nonlinear Sciences* (Cambridge University Press, Cambridge, 2001).

[3] E. S. Morse, Fireflies flashing in unison, Science **48**, 92 (1918).

[4] M. H. Hastings and E. D. Herzog, Clock genes, oscillators, and cellular networks in the suprachiasmatic nuclei, J. Biol. Rhythms **19**, 400 (2004).

[5] D. M. Abrams and S. H. Strogatz, Chimera States for Coupled Oscillators, Phys. Rev. Lett. **93**, 174102 (2004).

[6] M. R. Tinsley, S. Nkomo, and K. Showalter, Chimera and phase-cluster states in populations of coupled chemical oscillators, Nat. Phys. **8**, 662 (2012).

[7] D. J. Watts and S. H. Strogatz, Collective dynamics of small-world networks, Nature (London) **393**, 440 (1998).

[8] X. F. Wang, Complex networks: topology, dynamics and synchronization, Int. J. Bifurcation Chaos **12**, 885 (2002).

[9] A. Arenas, A. Diaz-Guilera, J. Kurths, Y. Moreno, and C. Zhou, Synchronization in complex networks, Phys. Rep. **469**, 93 (2008).

[10] M. G. Rosenblum, A. S. Pikovsky, and J. Kurths, Phase Synchronization of Chaotic Oscillators, Phys. Rev. Lett. **76**, 1804 (1996).

[11] Y. Kuramoto, *Chemical Oscillations, Waves, and Turbulence* (Courier, New York, 2003).

[12] J. J. Hopfield, Neural networks and physical systems with emergent collective computational abilities, Proc. Natl. Acad. Sci. (USA) **79**, 2554 (1982).

[13] E. J. Furshpan and D. D. Potter, Transmission at the giant motor synapses of the crayfish, J. Physiol. **145**, 289 (1959).

[14] P. Phelan, L. A. Goulding, J. L. Tam, M. J. Allen, R. J. Dawber, J. A. Davies, and J. P. Bacon, Molecular mechanism of rectification at identified electrical synapses in the Drosophila giant fiber system, Curr. Biol. **18**, 1955 (2008).

[15] M. F. Nolan, S. D. Logan, and D. Spanswick, Electrophysiological properties of electrical synapses between rat sympathetic preganglionic neurones in vitro, J. Physiol. **519**, 753 (1999).

[16] L. C. Barrio, T. Suchyna, T. Bargiello, L. X. Xu, R. S. Roginski, M. V. Bennett, and B. J. Nicholson, Gap junctions formed by connexins 26 and 32 alone and in combination are differently affected by applied voltage, Proc. Natl. Acad. Sci. (USA) **88**, 8410 (1991).

[17] A. T. Winfree, Spiral waves of chemical activity, Science **175**, 634 (1972).

[18] G. Ertl, Reactions at surfaces: from atoms to complexity (Nobel Lecture), Angew. Chem. Intl. Ed. **47**, 3524 (2008).

[19] C. Fernandez-Oto, D. Escaff, and J. Cisternas, Spiral vegetation patterns in high-altitude wetlands, Ecol. Complex. **37**, 38 (2019).

[20] J. Christoph, M. Chebbok, C. Richter, J. Schröder-Schetelig, P. Bittihn, S. Stein, I. Uzelac, F. H. Fenton, G. Hasenfuß, R. F. Gilmour, and S. Luther, Electromechanical vortex filaments during cardiac fibrillation, Nature (London) **555**, 667 (2018).

[21] X. Huang, W. Xu, J. Liang, K. Takagaki, X. Gao, and J.-Y. Wu, Spiral wave dynamics in neocortex, Neuron **68**, 978 (2010).

[22] J. J. Tyson and J. P. Keener, Singular perturbation theory of traveling waves in excitable media (a review), Physica D **32**, 327 (1988).

[23] M. Sutthiopad, J. Luengviriya, P. Porjai, M. Phantu, J. Kanchanawarin, S. C. Müller, and C. Luengviriya, Propagation of spiral waves pinned to circular and rectangular obstacles, Phys. Rev. E **91**, 052912 (2015).

[24] N. Wiener and A. Rosenblueth, The mathematical formulation of the problem of conduction of impulses in a network of connected excitable elements, specifically in cardiac muscle, Arch. Inst. Cardiol. Mex. **16**, 205 (1946).

[25] O. Steinbock and S. C. Müller, Chemical spiral rotation is controlled by light-induced artificial cores, Physica A **188**, 61 (1992).

[26] O. Steinbock, P. Kettunen, and K. Showalter, Anisotropy and spiral organizing centers in patterned excitable media, Science **269**, 1857 (1995).

[27] H. Ke, Z. Zhang, and O. Steinbock, Pinned chemical waves in the presence of Stokes flow, J. Phys. Chem. A **118**, 6819 (2014).

[28] B. T. Ginn and O. Steinbock, Quantized Spiral Tip Motion in Excitable Systems with Periodic Heterogeneities, Phys. Rev. Lett. **93**, 158301 (2004).

[29] Z. A. Jiménez and O. Steinbock, Stationary Vortex Loops Induced by Filament Interaction and Local Pinning in a Chemical Reaction-Diffusion System, Phys. Rev. Lett. **109**, 098301 (2012).

[30] D. Barkley, A model for fast computer simulation of waves in excitable media, Physica D **49**, 61 (1991).

[31] J. Löber and H. Engel, Analytical approximations for spiral waves, Chaos **23**, 043135 (2013).

[32] See Supplemental Material at http://link.aps.org/supplemental/10.1103/PhysRevE.103.022213 for supplementary animations that complement Figs. 1(e)–1(i), 2, 6(a), and 6(b).

[33] J. D. Dockery, J. P. Keener, and J. J. Tyson, Dispersion of traveling waves in the Belousov-Zhabotinskii reaction, Physica D **30**, 177 (1988).

[34] J.-M. Flesselles, A. Belmonte, and V. Gáspár, Dispersion relation for waves in the Belousov-Zhabotinsky reaction, J. Chem. Soc. Faraday Trans. **94**, 851 (1998).

[35] T. Erneux, *Applied Delay Differential Equations* (Springer, New York, 2009).

[36] I. R. Epstein and Y. Luo, Differential delay equations in chemical kinetics. Nonlinear models: the cross-shaped phase diagram and the Oregonator, J. Chem. Phys. **95**, 244 (1991).

[37] M. R. Roussel, The use of delay differential equations in chemical kinetics, J. Phys. Chem. **100**, 8323 (1996).

[38] R. Hinch and S. Schnell, Mechanism equivalence in enzyme-substrate reactions: distributed differential delay in enzyme kinetics, J. Math. Chem. **35**, 253 (2004).

[39] V. Krinsky and K. Agladze, Interaction of rotating waves in an active chemical medium, Physica D **8**, 50 (1983).

[40] U. Parlitz, A. Schlemmer, and S. Luther, Synchronization patterns in transient spiral wave dynamics, Phys. Rev. E **83**, 057201 (2011).

[41] N. Manz, C. T. Hamik, and O. Steinbock, Tracking Waves and Vortex Nucleation in Excitable Systems with Anomalous Dispersion, Phys. Rev. Lett. **92**, 248301 (2004).